M. Alizadeh, M. Mirak, E. Salahinejad, M. Ghaffari, R. Amini, A. Roosta, *Structural characterization of electro-codeposited Ni–*Al_2O_3*–SiC nanocomposite coatings*, Journal of alloys and compounds, 611 (2014) 161-166.
https://doi.org/10.1016/j.jallcom.2014.04.181

Structural characterization of electro-codeposited Ni-Al_2O_3-SiC nanocomposite coatings

M. Alizadeh [a,*], M. Mirak [a], E. Salahinejad [b], M. Ghaffari [c,d], R. Amini [a], A. Roosta [e]

[a] Department of Materials Science and Engineering, Shiraz University of Technology, Shiraz, Iran

[b] Faculty of Materials Science and Engineering, K.N. Toosi University of Technology, Tehran, Iran

[c] Department of Electrical and Electronics Engineering, UNAM-National Institute of Materials Science and Nanotechnology, Bilkent University, Ankara, Turkey

[d] Young Researchers Club, Islamic Azad University, Najafabad Branch, Isfahan, Iran

[e] Chemical Engineering, Petroleum and Gas Department, Shiraz University of Technology, Shiraz, Iran

Abstract

In this study, nanostructured Ni-Al_2O_3-SiC composite and pure nickel coatings were prepared by co-electrodeposition from a modified Watt's type bath, with and without adding nanosized Al_2O_3 and SiC particles, respectively. The structure of the coatings was studied by using X-ray diffraction, scanning electron microscopy, and transmission electron microscopy. The composition of the coatings was also evaluated by energy dispersive X-ray spectroscopy. The results confirmed the presence of a face centered cubic crystalline structure of the Ni matrix for both of the deposition routes. It was also found that the morphology of the pure nickel coating is uniform, whereas the Ni-Al_2O_3-SiC nanocomposite coatings indicate a

---

[*] **Corresponding Author:** *Email address*: Alizadeh@sutech.ac.ir (Morteza Alizadeh)

protrusive and heterogeneous morphology. Moreover, the incorporation of the nanoparticles significantly affected the crystallite size of the Ni matrix.

Keywords: Coating materials; Composite materials; Microstructure

1. Introduction

In the recent decades, various techniques like physical vapor deposition, chemical vapor deposition, laser beam deposition, ion implantation, plasma jet, and electrodeposition have been developed to synthesize composite coatings [1-6]. Among these methods, electrodeposition is a valuable production method, because the wide range of substrate sizes and shapes can be cost-effectively coated by this technique [7-9]. Recently, this method has been used to produce nanostructured metal-matrix composite coatings, being composed of the matrices of nickel, copper, cobalt, silver, etc and the ceramic reinforcements of TiO_2, Al_2O_3, SiO_2, B_4C, SiC, etc.

The presence of ceramic nanoparticles in coatings improves some properties like hardness, wear, and corrosion resistance [9]. The improvement of these properties depends mainly on the size and percentage of the co-deposited particles and the particle distribution in the metallic matrix [8]. The amount and distribution of the particles during metal electrodeposition depend on a variety of working parameters, such as bath composition, pH, temperature, and current density [10-12]. It is noticeable that nanoparticles tend to agglomerate in the plating bath, due to their high surface energy and the high ionic concentration of the plating bath [12]; hence, the deposition of the high levels of non-agglomerated, finely dispersed particles is a main challenge. In this regard, some studies have been performed to restrain the agglomeration of nanoparticles [12].

This is the accepted manuscript (postprint) of the following article:
M. Alizadeh, M. Mirak, E. Salahinejad, M. Ghaffari, R. Amini, A. Roosta, *Structural characterization of electro-codeposited Ni–Al_2O_3–SiC nanocomposite coatings*, Journal of alloys and compounds, 611 (2014) 161-166.
https://doi.org/10.1016/j.jallcom.2014.04.181

There are some papers in the literature focusing on the effect of matrix and reinforcement on the microstructure, mechanical properties, and corrosion behavior of the composite coatings produced by the electrodeposition method [13-17]. Most researchers have used nickel as the matrix and a wide range of oxide and carbide ceramic particles as the reinforcement [13-17]. For instance, Borkar et al. [18] successfully produced Ni/SiC nanocomposite coatings and showed that the microhardness and wear resistance of the Ni/SiC composite coatings are improved by increasing the SiC content. Moreover, the corrosion and oxidation resistance is improved via the incorporation of Al_2O_3 nanoparticles into the Ni matrix [18]. As it was seen, each of the ceramic particles induces a special property in the matrix. For example, some of the ceramic particles improve mechanical properties and some improve the corrosion behavior of the coating; hence, it is expected that the most desirable properties can be obtained by the addition of two or more types of ceramic particles.

To the best of our knowledge, no comprehensive study has been reported that benefits from both of the Al_2O_3 and SiC properties by co-electrodeposition of metal matrix composite coatings. Investigations on the components design, preparation technology, microstructures, and properties of multi-component nanocomposite coatings have rarely been reported, due to the existing problems of complexity of multi-elemental electrodeposition [19-23]. In the present study, Ni-Al_2O_3-SiC nanocomposite coatings were produced by the electrodeposition method using a Watt type bath containing mechanically-dispersed Al_2O_3-SiC nanoparticles. The effects of the nanoparticles concentration in the electrolyte on the microstructure of the nanocomposite coatings were investigated.

2. Experimental procedure

M. Alizadeh, M. Mirak, E. Salahinejad, M. Ghaffari, R. Amini, A. Roosta, *Structural characterization of electro-codeposited Ni–Al_2O_3–SiC nanocomposite coatings*, Journal of alloys and compounds, 611 (2014) 161-166.
https://doi.org/10.1016/j.jallcom.2014.04.181

2.1. Electrode pre-treatment and electrolyte preparation

Pure nickel (99.99%) plates (60 mm×35 mm×6 mm) were used as the anode. The cathode was a stainless steel plate with the size of 20 mm×16 mm×1.5 mm. The surface area of the anode was chosen approximately five times greater than that of the cathode to ensure that no problem arises from the anodic polarization of nickel. Prior to the electrodeposition process, the substrate was mechanically polished with emery papers to No. 2000, sonicated in acetone for about 10 min, and then activated in 10% hydrochloric acid for about 5 min at room temperature.

2.2. Electrolyte preparation and optimization

In this work, many attempts were made to determine the optimum bath composition and conditions for electrodeposition of a Ni–Al_2O_3-SiC layer. The composition of the electrolyte bath was based on a modified Watts Ni bath, as listed in Table 1. The solution was prepared from analytic grade chemicals and double distilled water. The average size of the Al_2O_3 and SiC particles (purity >99.9%) was about 40 and 45 nm, respectively. Nanosized Al_2O_3 and SiC particles in different concentrations (0-12.5 g l^{-1}) were added to the bath with 1:1 ratio. A surfactant was also added to the electrolyte in order to distribute the deposited nickel in a more uniform fashion. Prior to the electrodeposition, the electrolyte bath was stirred for about 24 h by using a magnetic stirrer at 1200 rpm to get de-agglomerate Al_2O_3-SiC nanoparticles. During the composite deposition process with parameters listed in Table 2, magnetic stirring was also employed to inhibit the precipitation of the particles and to keep the electrolyte fresh. Both of the electrodes were dipped in 500 ml of the test electrolyte dispersions.

2.3. Microstructural characterization

A Vega-XMU scanning electron microscope (SEM) was used to observe and investigate the surface morphology and map micrographs of the Ni-Al_2O_3-SiC coatings co-deposited by the different concentrations of the ceramic particles. The composition of the coatings was also examined by an energy dispersive X-ray spectroscopy (EDS) attached to the SEM, over three uniform regions.

The crystal structure of the composite coatings was examined by using X-ray diffraction (XRD, D8 Bruker diffractometer) with Cu $K\alpha_1$ radiation ($\lambda = 0.15406$ nm) in the range of $2\theta = 20\text{-}100°$ in a step size of 0.03° and a counting time of 3s per step. The XRD quantitative analysis was done by the Rietveld method. Additionally, the microstructure of the coatings was studied by a high resolution transmission electron microscope (HRTEM, FEI, Tecnai G2 F30). For the TEM examination, the nanocomposite coating was peeled off from the substrate and a foil of 3 mm in diameter was obtained using a disc punch. It was further thinned by an ion polishing system.

3. Results and discussion

3.1. XRD studies

The phase composition and structure of the pure Ni and Ni-Al_2O_3-SiC coatings with the different Al_2O_3-SiC contents in the bath were investigated by XRD. Fig. 1 depicts the XRD patterns of the pure Ni and Ni-Al_2O_3-SiC composite coatings obtained at a current density of 1 Adm^{-2}. As can be seen, the majority of the XRD peaks are related to Ni with a FCC crystalline structure, albeit with different orientations influenced by the particle content.

M. Alizadeh, M. Mirak, E. Salahinejad, M. Ghaffari, R. Amini, A. Roosta, *Structural characterization of electro-codeposited Ni–Al_2O_3–SiC nanocomposite coatings*, Journal of alloys and compounds, 611 (2014) 161-166.
https://doi.org/10.1016/j.jallcom.2014.04.181

The peaks observed in the diffractograms of the Ni-Al_2O_3-SiC composite coatings at the angles of about 44.5°and 51.98° correspond to the (111) and (200) planes of Ni, respectively. The deposition of Ni from the Watt type bath results in the crystallites growing predominantly in the direction of the (111) plane [1]. The co-deposition of the Al_2O_3 and SiC particles obviously affects the relative intensity of the different crystal planes. As can be seen from Fig. 1, by increasing the Al_2O_3 and SiC content in the coatings, the relative peak intensity of the crystal planes of (1 1 1) and (2 0 0) is decreased [16]. The small peaks at about 35° in Fig. 1 correspond to Al_2O_3. There is no distinguished reflection of SiC at the amounts of 5 and 15 g l^{-1}, which is attributed to the low content of the SiC particles in the coatings. Nevertheless, a SiC peak is observed in the Ni-Al_2O_3-SiC (25 g l^{-1}) coating at 2θ about 38°. According to Fig .1, the diffraction peak broadening of the Ni-Al_2O_3-SiC nanocomposite coatings in the 25 g l^{-1} electrolyte is more than that 5 and 15 g l^{-1}. This behavior is attributed to a decrease in the nickel crystallite size, due to the co-deposition of the nanoparticles in the nickel matrix.

3.2. Effect of the particles concentration in the electrolyte and the particles content in the deposits

The effect of the concentration of the Al_2O_3 and SiC nanoparticles in the electrolyte bath on the content of the co-deposited Al_2O_3 and SiC nanoparticles is shown in Fig. 2. Each point of the figure has been extracted from the average value of three EDX measurements at different locations on each of the coated sample. The evaluation of this figure shows that the weight percent of the co-deposited particles continuously increases with increasing the Al_2O_3 and SiC nanoparticles concentration in the electrolyte. An increase in the concentration of the

Al_2O_3 and SiC nanoparticles in the plating bath enhances their adsorption rate; as a result, a higher weight percentage of the nanoparticles are co-deposited. For example, the weight percentage of the co-deposited nanoparticles is about 3.5 wt.% corresponding to 5 g l^{-1} of the nanoparticles in the bath, while it is 7.35 wt.% in 25 g l^{-1} bath. If the reinforcement particles are saturated in the composite coating, the screening effect of the formed composite coating may appears, which might result in weakening of the electrostatic attraction between the substrate and the suspended reinforcement particles in the nickel bath [24]. There are two reasons for the decrease of the particle content in the coating beyond the optimum value of the particles in the electrolyte: (a) the particles concentration beyond the optimum value in the electrolyte can lead to a barrier effect for the particles co-deposited in the matrix. Because of elastic collisions between the particles inside the electrolyte, some of the particles are recrudesced from the interface between the electrolyte and substrate, where the particle density is the highest. Therefore, the particles are reduced in the matrix [25], (b) Despite the fact that the number of the reinforcement particles approaching the cathode surface are increased by the reinforcement content increase in the plating bath, the capturing capacity of the growing metal matrix remains virtually constant [26]; as a result, a longer period is required for the nanoparticles to be imbedded into the Ni matrix metal. The attachment of the nanoparticles to the coatings and then the increase of them can be explained by the following mechanism:

At first, the present particles in the electrolyte are carried by a net positive charge which facilitates their migration towards the negatively-charged steel substrate surface [27]. Afterwards, the nanoparticles are co-deposited by a two-step adsorption model. In the first step, the particles are adsorbed loosely on the electrode surface and remain in equilibrium with the particles in the solution [28]. The particles are still surrounded by a thin layer of adsorbed ions and solvent molecules, affecting the interaction between the particles and electrode. In the second step, the layer of ions adsorbed at the interface collapses by the electrical field, followed by a strong adsorption of the particles onto the electrode.

As can be seen from Fig. 2, the weight percentage of the Al_2O_3 nanoparticles in the coatings is more than that of the SiC nanoparticles, while the ratio of the Al_2O_3 and SiC particles in the electrolyte bath is equal for all of the bath concentrations. This is because of the higher activity of Al_2O_3 in comparison to the SiC particles in bonding to the Ni matrix [18]. It should be noted that the mechanism of this behavior is not exactly known and it seems to be a function of different sizes/densities of the nanoparticles, surface properties (hydrophobicity/hydrophilicity, zeta potential), and their interactions with the ions in the electrolyte bath [18].

3.3. Surface morphology and composition

The effect of the reinforcement content in the electrolyte on the morphology of the Ni matrix is depicted in Fig. 3. The micrographs show the surface morphology of the pure Ni and Ni–Al_2O_3-SiC nanocomposite coatings containing 5, 15 and 25 g l^{-1} Al_2O_3-SiC nanoparticles. As can be seen, the morphology of the pure nickel coating is uniform and has grown along a preferred orientation, which is compatible with the literature [29]. The morphology of the coatings changes after the addition of the Al_2O_3-SiC nanoparticles. Also, the morphology of the coatings in the various contents of the nanoparticles is different. Fig. 3(b) shows that the morphology of the Ni–Al_2O_3-SiC (5 g l^{-1}) composite coating is fine and the deposit has a heterogeneous surface. The morphology of the Ni -Al_2O_3-SiC (15 and 25 g

l^{-1}) composite coatings is more heterogeneous and the protruding points are clearly visible, as shown by an arrow. It has been reported that by adding reinforcement nanoparticles to Ni coatings, the grain morphology of coarse polyhedral Ni crystallites would change into protruding crystallite morphology. The change in the morphology can be related to the change of the preferred orientation in pure Ni into randomly-oriented composite deposits [29]. However, the morphology of the Ni-Al_2O_3-SiC composite coatings in all of the reinforcement particle contents is heterogeneous, where heterogeneity in the surface morphology increases with the amount of the particles in the bath. It should be noted that the incorporation of the Al_2O_3-SiC nanoparticles to the Ni matrix leads to a compact structure, as reported by Ruidong et al. [30].

In the initial stage of the electrodeposition process, nickel ions are deposited preferably on the substrate and a nickel layer is produced. Afterwards, the ceramic particles and nickel ions are deposited simultaneously on the growing metal matrix [31]. The nickel electrodeposition process from the Watt's solution consists of a multi-step reaction, typically two successive electron transfer steps. The electrode reactions are shown as follows:

$$Ni^{+2} + H_2O \longrightarrow NiOH^+ + H^+ \tag{1}$$

$$NiOH^+ + e^- \longrightarrow NiOH_{(ads)} \tag{2}$$

$$NiOH^+ + NiOH_{(ads)} + 3e^- \longrightarrow 2Ni + 2OH^- \tag{3}$$

In the electrodeposition process, the boric acid which is in the electrolyte bath reacts and gets ionized according to the following reaction:

$$B(OH)_3 + H_2O \longrightarrow [B(OH)_4]^- + H^+ \tag{4}$$

Al_2O_3 and SiC nanoparticles in the electrolyte adsorb Ni^{2+}, $Ni\,[B(OH)_4]^+$, Na^+, and sodium dodecyl sulphate ions and are then attached to the adsorbed Ni ions. The particles along with the adsorbed cations migrate towards the growing Ni matrix [26, 32]. The presence of the Al_2O_3 and SiC nanoparticles in the coating prevents the further growth of the Ni grains, due to the following factors: (i) the increase of the number of nucleation sites, (ii) the postponed growth of Ni grains, (iii) the change in the preferred growth orientations for grains [26, 32]. It has been reported that when ceramic particles are in a Watt's type bath solution, a charged layer can be generated on the ceramic particles surface, due to the adsorption of hydrogen ions and nickel hydration positive ions [33, 34]. The charged particles are absorbed on the matrix surface and act as nickel crystallite nucleation sites. Therefore, the nucleation rate of crystallites is faster than their growth rate, causing a grain refinement. The increase of ceramic particles (in this work, Al_2O_3 and SiC) in the coatings provides a large amount of nucleation sites on the coating, and the grain refinement occurs more strongly. The crystallite size of the nanocrystalline composite coatings was calculated by the FWHM of the prominent (111) reflection by the Scherer's Equation. The effect of the particle concentration on the nickel deposited crystallite size is demonstrated in Fig 4. According to the figure, the average crystallite size of pure nickel is 32.5 nm, whereas the addition of the nanoparticles resulted in a decrease in the crystallite size to 14.3 nm corresponding to the coating co-deposited in 25 g l^{-1}. As Fig. 4 shows, a sharp decrease in the crystallite size of pure Ni is observed by adding the nanoparticles, even at the small amount of the reinforcement in the bath, which is related to the effect of the nanoparticles embedded in the deposited layer on the nucleation rate of the crystallites.

The cross-sectional SEM morphology of the Ni–Al_2O_3-SiC nanocomposite coating is shown in Fig. 5. It is shown that the coating shows a compact structure, and no defect is observed at the steel substrate/layer interface, suggesting that a appropriate bonding between the coating and substrate. Also, as can be seen in Fig. 5, a uniform distribution of the nanoparticles has been achieved in the nanocomposite coating, which implies that rotation generated by magnetic stirring during electrodeposition has shattered the agglomerated particles. Considering Fig. 5, the coating thickness was measured to be approximately 40 µm. The deposition rate for the pure Ni specimen was measured to be 0.92 m/h, while the deposition rate of the Ni-Al_2O_3-SiC specimen decreased to 0.75 m/h. This could be due to the fact that the addition of the Al_2O_3 and SiC particles and the surfactant into the solution caused the covering of the cathode surface, preventing the diffusion of the Ni^{2+} ions towards the interface and preventing the co-deposition [10].

The typical EDS analysis related to 25 g l^{-1} Al_2O_3 and SiC nanoparticles suspended in the bath is depicted in Fig. 6. The peaks located at 0.21, 1.54, 1.83 and 7.95 keV are attributed to O, Al, Si and Ni, respectively. The intensity of the peaks indicates that the weigh percent of Ni is more than that of Si and Al, despite the fact that the EDS micrograph that has been extracted from a part in which the nanoparticles are deposited. This shows that Ni is a basic element in the coatings.

The elemental EDS map of the Ni-Al_2O_3-SiC nanocomposite coating that corresponds to 25 g l^{-1} nanoparticles on the coating surface and the related micrograph are shown in Fig. 7. As can be seen, a uniform distribution of the elements in the coating has been produced. The association of secondary electron (SE) analysis with a related elemental map illustrates that the nanoparticles are seen as dark spots in the bright Ni matrix. The comparison of the map of Al and Si reveals that the adsorbed Al_2O_3 content in the coating is more than the SiC content, which confirms the result presented in Fig 1.

This is the accepted manuscript (postprint) of the following article:
M. Alizadeh, M. Mirak, E. Salahinejad, M. Ghaffari, R. Amini, A. Roosta, *Structural characterization of electro-codeposited Ni–Al_2O_3–SiC nanocomposite coatings*, Journal of alloys and compounds, 611 (2014) 161-166.
https://doi.org/10.1016/j.jallcom.2014.04.181

Fig. 8 shows the bright-field transmission electron microscopy image of the Ni-Al_2O_3-SiC nanocomposite coating at 25 g l^{-1} nanoparticles. As can be seen, the nanoparticles can be observed in the coating. The black sections in Fig. 8 are nanoparticles, where the average diameter is approximately 40 nm. According to this figure, the nanoparticles are strongly embedded into the nickel matrix since no crack or hole is observed.

4. Conclusions

In this study, the structure of pure Ni and Ni-Al_2O_3-SiC nanocomposite coatings deposited on a steel substrate via the co-electrodeposition process were investigated. The outcome of this study can be summarized as follows:

1. The XRD analysis showed that the Ni-Al_2O_3-SiC nanocomposite was successfully produced by the electrodeposition process.

2. The weight percent of the co-deposited particles is continuously increased by increasing the Al_2O_3 and SiC nanoparticles concentration in the electrolyte.

3. The addition of the Al_2O_3 and SiC nanoparticles to the Ni matrix affected the microstructure of the coating and changed polyhedral Ni crystallites to a protrusilited crystallite morphology.

4. The crystallite size of the composite coatings decreased with increasing the Al_2O_3-SiC content in the electrolyte and reached the minimum value of 14.3 nm at 25 g l^{-1}, which was 2.3 times lower than that of the pure nickel coatings.

5. Elemental mapping on the surface showed that the Al_2O_3 and SiC nanoparticles were homogeneously distributed in the Ni matrix.

M. Alizadeh, M. Mirak, E. Salahinejad, M. Ghaffari, R. Amini, A. Roosta, *Structural characterization of electro-codeposited Ni–Al_2O_3–SiC nanocomposite coatings*, Journal of alloys and compounds, 611 (2014) 161-166.
https://doi.org/10.1016/j.jallcom.2014.04.181

5. Acknowledgement

The authors gratefully acknowledge the financial support received from the Iran National Science Foundation (INSF).

Reference

[1] S. Ghanbari, F. Mahboubi, Corrosion resistance of electrodeposited Ni–Al composite coatings on the aluminum substrate, Mater. Des. 32 (2011) 1859-1864.

[2] N. Daemi, F. Mahboubi, H. Alimadadi, Effect of plasma nitriding on electrodeposited Ni–Al composite coating, Mater. Des. 32 (2011) 971-975.

[3] P. Gyftou, E.A. Pavlatou, N. Spyrellis, Effect of pulse electrodeposition parameters on the properties of Ni/nano-SiC composites, Appl. Surf. Sci. 254 (2008) 5910–5916.

[4] A. Dasgupta, P. Kuppusami, F. Lawrence, V.S. Raghunathan, P.A. Premkumar, K.S. Nagaraja, Plasma assisted metal-organic chemical vapor deposition of hard chromium nitride thin film coatings using chromium(III) acetylacetonate as the precursor, Mater. Sci. Eng. A. 374 (2004) 362-368.

[5] A.D Pogrebnjak, Sh.M. Ruzimov, D.L. Alontseva, P. Zukowski, C. Karwat, C. Kozak, M. Kolasik, Structure and properties of coatings on Ni base deposited using a plasma jet before and after electron a beam irradiation, Vacuum 81 (2007) 1243-1251.

[6] Y.X. Chen, W.M. Liu, C.F. Ye, S.K. Qi, Preparation and characterization of self-assembled alkanephosphate monolayers on glass substrate coated with nano-TiO_2 thin film, Mater. Res. Bull. 36 (2001) 2605-2612.

[7] M. Lekka, D. Koumoulis, N. Kouloumbi, P.L. Bonora, Mechanical and anticorrosive properties of copper matrix micro- and nano-composite coatings, Electrochim. Acta 54 (2009) 2540-2546.

[8] B. Losiewicz, A. Stepien, D. Gierlotka, A. Budniok, Composite layers in Ni–P system containing TiO$_2$ and PTFE, Thin Solid Films 349 (1999) 43-50.

[9] D.F. Susan, K. Barmak, A.R. Marder, Electrodeposited Ni-Al particle composite coatings, Thin Solid Films 307 (1997) 133-140.

[10] S.R. Allahkaram, S. Golroh, M. Mohammadalipour, Properties of Al$_2$O$_3$ nano-particle reinforced copper matrix composite coatings prepared by pulse and direct current electroplating, Mater. Des. 32 (2011) 4478-4484.

[11] Z.F. Lodhi, J.M.C. Mol, A. Hovestad, H. Terryn, J.H.W. de Wit, Electrodeposition of Zn–Co and Zn–Co–Fe alloys from acidic chloride electrolytes, Surf. Coat. Technol. 202 (2007) 84-90.

[12] R. Sen, S. Bhattacharya, S. Das, K. Das, Effect of surfactant on the co-electrodeposition of the nano-sized ceria particle in the nickel matrix, J. Alloys Compd. 489 (2010) 650-658.

[13] D. Thiemig, A. Bund, Characterization of electrodeposited Ni–TiO$_2$ nanocomposite coatings, Surf. Coat. Technol. 202 (2008) 2976-2984.

[14] Zh. Zengwei, Zh. Di, Q. Ningsong, L. Weining, Electrodeposition of bright nickel coating under perturbation of hard particles, Mater. Des. 28 (2007) 1776-1779.

[15] B. Ranjith, G.P. Kalaignan, Ni–Co–TiO$_2$ nanocomposite coating prepared by pulse and pulse reversal methods using acetate bath, Appl. Surf. Sci. 257 (2010) 42-47.

[16] C.C. Anya, Wet erosive wear of alumina and its composites with SiC nano-particles, Ceram. Int. 24 (1998) 533-542.

[17] Z. Wang, J. Shemilt, P. Xiao, Novel fabrication technique for the production of ceramic/ceramic and metal/ceramic composite coatings, Scrip. Mater. 42 (2000) 653-659.

[18] T. Borkar, S.P. Harimkar, Effect of electrodeposition conditions and reinforcement content on microstructure and tribological properties of nickel composite coatings, Surf. Coat. Technol. 205 (2011) 4124-4134.

[19] L. Dengyou, L. Qimei, W. Huixian, C. Jinhua, Direct synthesis of micro-coiled carbon fibers on graphite substrate using co-electrodeposition of nickel and sulfur as catalysts, Mater. Des. 30 (2009) 649-652.

[20] G. Zhong-cheng, X. Rui-dong, Z. Xiao-yun, Studies on the wear resistance and the structure of electrodeposited RE-Ni-W-P-SiC-PTFE composite materials, Surf. Coat. Technol. 187 (2004) 141-145.

[21] X. Rui-dong, W. Jun-li, H. Li-fang, G. Zhong-cheng, Study on the characteristics of Ni–W–P composite coatings containing nano-SiO_2 and nano-CeO_2 particles, Surf. Coat. Technol. 202 (2008) 1574-1579.

[22] S. Yue-hai, W. Gang, W. Rong-chun, Properties and structure of RE-Ni-W-P-SiC composite coating prepared by impulse electrodeposition, Trans. Nonferr. Metal. Soc. 17 (2007) 363-367.

[23] L. Shi, C. Sun, P. Gao, F. Zhou, W. Liu, Mechanical properties and wear and corrosion resistance of electrodeposited Ni–Co/SiC nanocomposite coating, Appl. Surf. Sci. 252 (2006) 3591-3599.

[24] I. ul Haq, T.I. Khan, Tribological behavior of electrodeposited Ni–SnO_2 nanocomposite coatings on steel, Surf. Coat. Technol., 205 (2011) 2871-2875.

[25] H. Gul, F. Kılıc, M. Uysal, S. Aslan, A. Alp, H. Akbulut, Effect of particle concentration on the structure and tribological properties of submicron particle SiC reinforced Ni metal matrix composite (MMC) coatings produced by electrodeposition, Appl. Surf. Sci. 258 (2012) 4260-4267.

[26] M. Srivastava, J.N. Balaraju, B. Ravishankar, K.S. Rajam, Improvement in the properties of nickel by nano-Cr_2O_3 incorporation, Surf. Coat. Technol. 205 (2010) 66-75.

[27] F.F. Xia, C. Liu, F. Wang, M.H. Wu, J.D. Wang, H.L. Fu, J.X. Wang, Preparation and characterization of Nano Ni–TiN coatings deposited by ultrasonic electrodeposition, J. Alloys. Compd. 490 (2010) 431-435.

[28] B.J. Hwang, C.S. Hwang, Mechanism of Codeposition of Silicon Carbide with Electrolytic Cobalt, J. Electrochem. Soc. 140 (1993) 979-984.

[29] L.P. Bicelli, B. Bozzini, C. Mele, L. D'Urzo, A review of nanostructural aspects of metal deposition, Int. J. Electrochem. Sci. 3 (2008) 356-408.

[30] M.R. Vaezi, S.K. Sadrnezhaad, L. Nikzad, Electrodeposition of Ni–SiC nano-composite coatings and evaluation of wear and corrosion resistance and electroplating characteristics, Coll. Surf. A. 315 (2008)176-182.

[31] L.B. Li, M.Z. An, G.H. Wu, Electroless deposition of nickel on the surface of silicon carbide/aluminum composites in alkaline bath, Mater. Chem. Phy. 94 (2005) 159-164.

[32] N.S. Qu, D. Zhu, K.C. Chan, Fabrication of Ni–CeO_2 nanocomposite by electrodeposition, Script. Mater. 54 (2006) 1421-1425.

[33] R. Sen, S. Bhattacharya, S. Das, K. Das, Effect of surfactant on the co-electrodeposition of the nano-sized ceria particle in the nickel matrix, J. Alloys. Compd. 489 (2010) 650–658.

M. Alizadeh, M. Mirak, E. Salahinejad, M. Ghaffari, R. Amini, A. Roosta, *Structural characterization of electro-codeposited Ni–Al_2O_3–SiC nanocomposite coatings*, Journal of alloys and compounds, 611 (2014) 161-166.
https://doi.org/10.1016/j.jallcom.2014.04.181

[34] I. Epelboin, M. Joussellin, R.J. Wiart, Impedance measurements for nickel deposition in sulfate and chloride electrolytes, Electroanal. Chem. 119 (1981) 61-71.

M. Alizadeh, M. Mirak, E. Salahinejad, M. Ghaffari, R. Amini, A. Roosta, *Structural characterization of electro-codeposited Ni–Al_2O_3–SiC nanocomposite coatings*, Journal of alloys and compounds, 611 (2014) 161-166.
https://doi.org/10.1016/j.jallcom.2014.04.181

Figures:

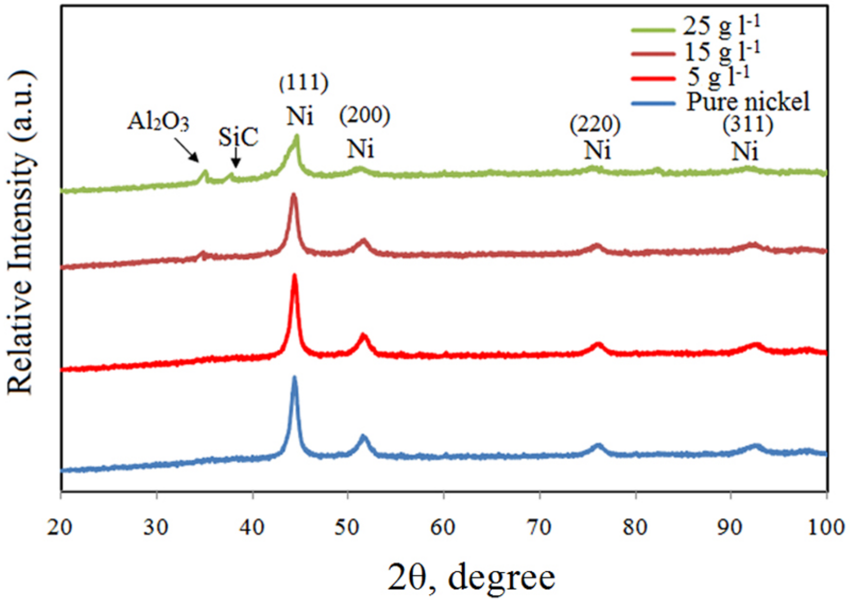

Fig.1. XRD patterns of the pure nickel and nanocomposite coatings.

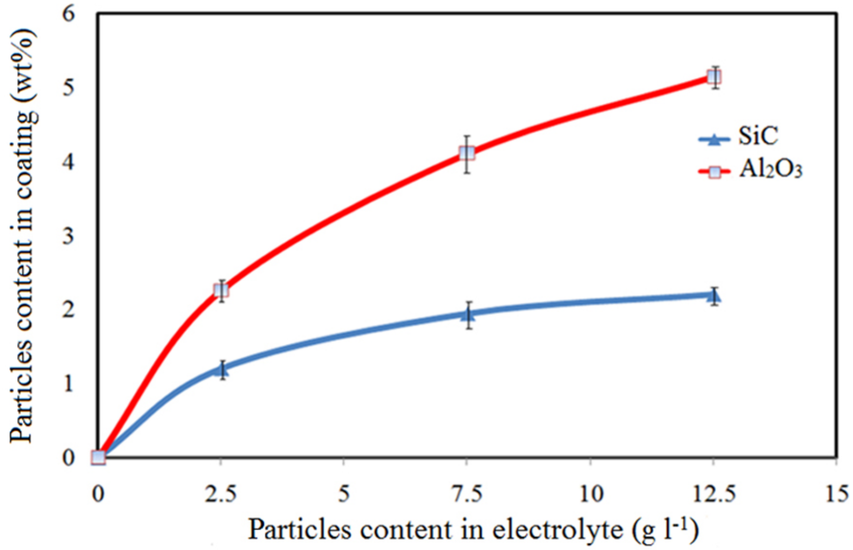

Fig. 2. Particle content in the coatings as a function of the concentration in the electrolyte bath.

M. Alizadeh, M. Mirak, E. Salahinejad, M. Ghaffari, R. Amini, A. Roosta, *Structural characterization of electro-codeposited Ni–Al_2O_3–SiC nanocomposite coatings*, Journal of alloys and compounds, 611 (2014) 161-166.
https://doi.org/10.1016/j.jallcom.2014.04.181

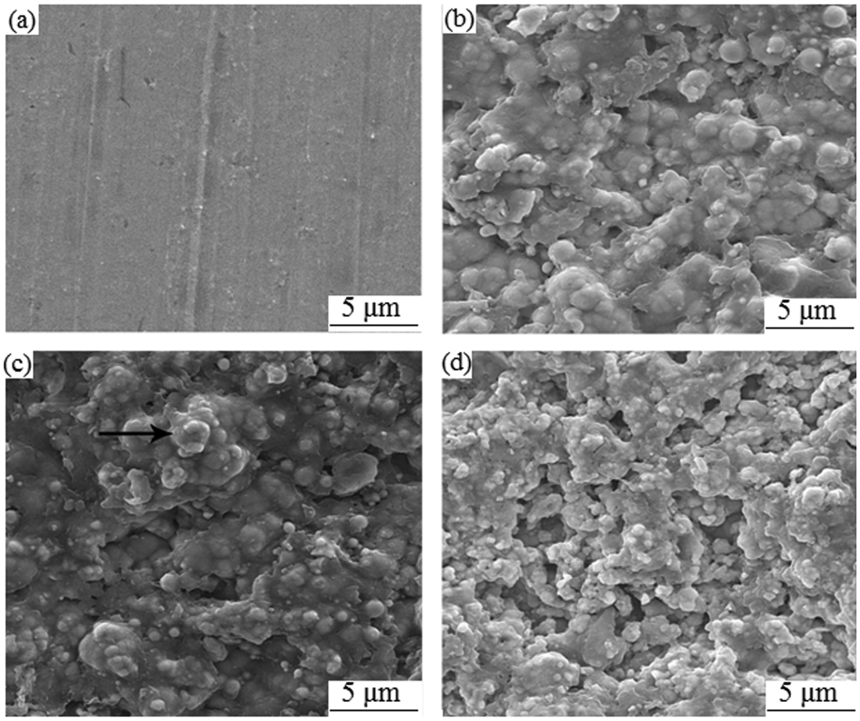

Fig. 3. SEM micrographs of the (a) pure nickel coating and the (b) Ni-Al_2O_3-SiC (5 g l^{-1}), (c) Ni-Al_2O_3-SiC (15 g l^{-1}), and (d) Ni-Al_2O_3-SiC (25 g l^{-1}) nanocomposite coatings.

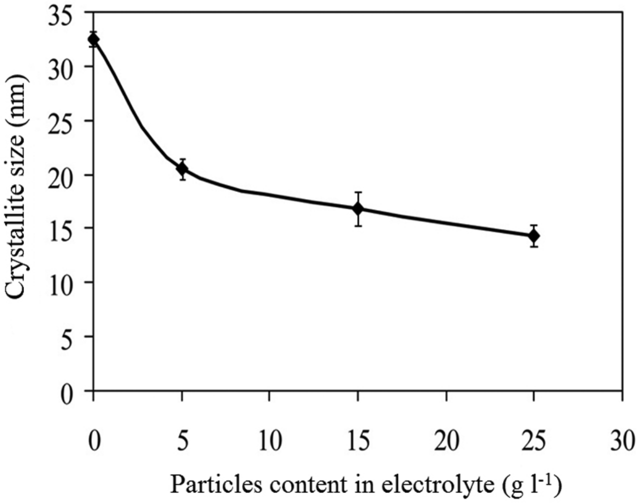

Fig. 4. Crystallite size of the Ni-Al_2O_3-SiC composite coatings as a function of the nanoparticles concentration in the electrolyte.

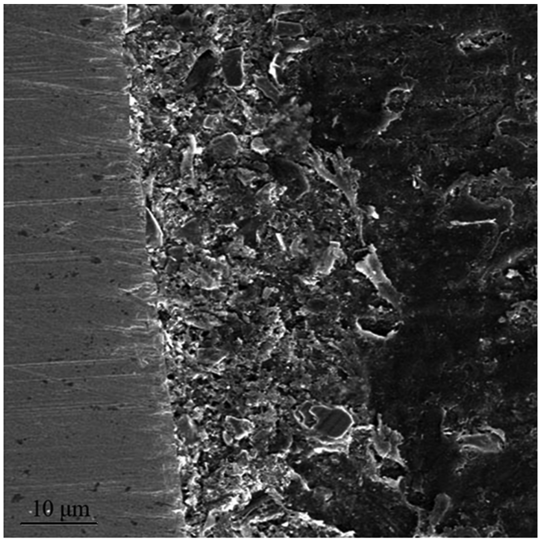

Fig. 5. Cross-sectional SEM morphology of the Ni-Al_2O_3-SiC (25 g l^{-1}) coating.

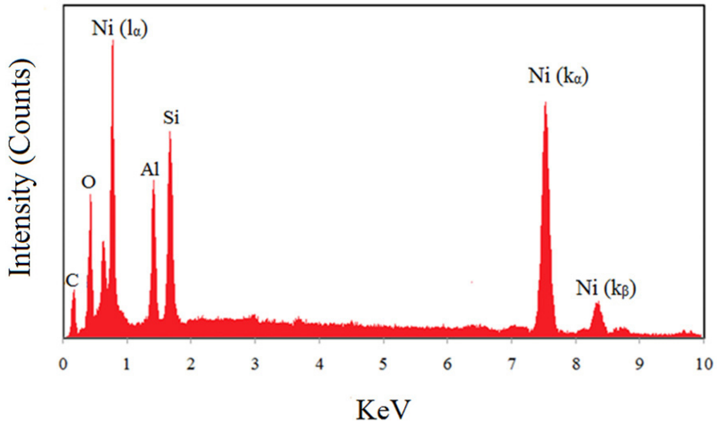

Fig. 6. EDS analysis of the Ni-Al_2O_3-SiC (25 g l^{-1}) coating.

M. Alizadeh, M. Mirak, E. Salahinejad, M. Ghaffari, R. Amini, A. Roosta, *Structural characterization of electro-codeposited Ni–Al_2O_3–SiC nanocomposite coatings*, Journal of alloys and compounds, 611 (2014) 161-166.
https://doi.org/10.1016/j.jallcom.2014.04.181

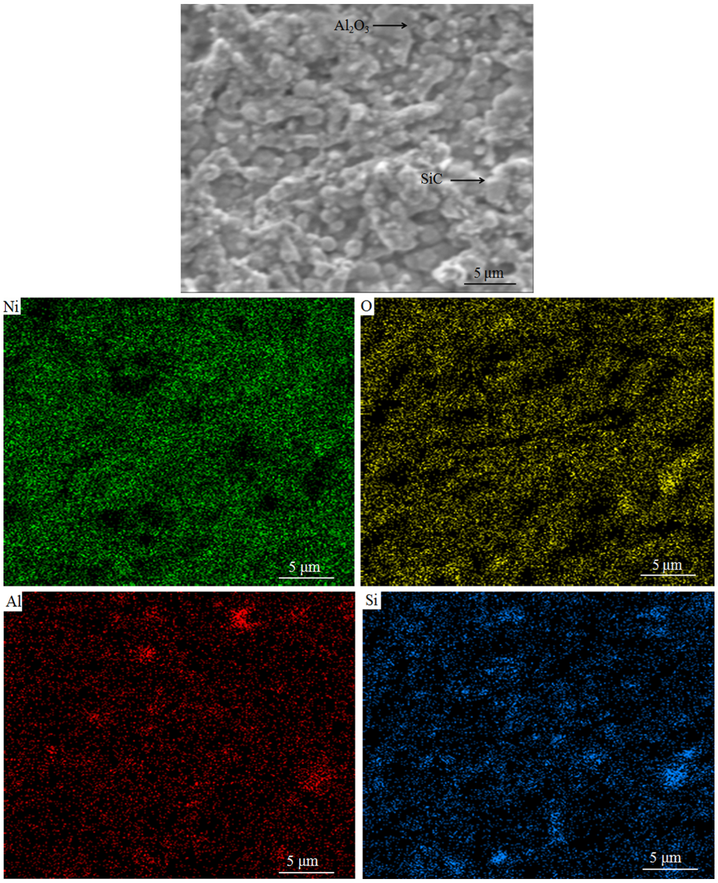

Fig. 7. Elemental X-ray maps of the Ni-Al_2O_3-SiC (25 g l^{-1}) nanocomposite coating.

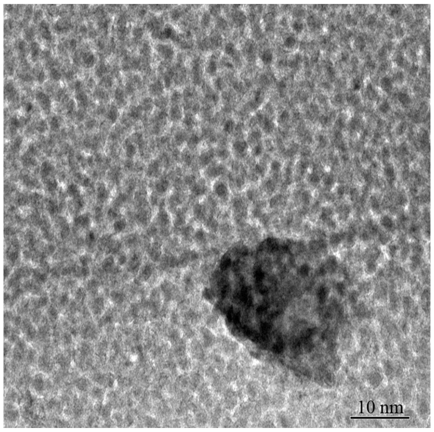

Fig. 8. Transmission electron microscopy micrograph of the Ni-Al_2O_3-SiC (25 g l^{-1}) nanocomposite coating.

M. Alizadeh, M. Mirak, E. Salahinejad, M. Ghaffari, R. Amini, A. Roosta, *Structural characterization of electro-codeposited Ni–Al_2O_3–SiC nanocomposite coatings*, Journal of alloys and compounds, 611 (2014) 161-166.
https://doi.org/10.1016/j.jallcom.2014.04.181

Tables:

Table 1. Bath composition.

Bath composition	$NiSO_4\cdot 6H_2O$	$NiCl_2\cdot 6H_2O$	H_3BO_3	$C_{12}H_{25}NaO_4S$ (SDS)	Al_2O_3 particle	SiC particles	Saccharin
Concentration (g l^{-1})	240	35	30	0.4	0-12.5	0-12.5	5

M. Alizadeh, M. Mirak, E. Salahinejad, M. Ghaffari, R. Amini, A. Roosta, *Structural characterization of electro-codeposited Ni–Al_2O_3–SiC nanocomposite coatings*, Journal of alloys and compounds, 611 (2014) 161-166.
https://doi.org/10.1016/j.jallcom.2014.04.181

Table 2. Electrodeposition conditions.

Current density (A dm^{-2})	Temperature (°C)	pH	Agitation speed (rpm)
1	45±1	3.7±0.2	250